Magnetic Fields for Cell Cultures Suspended in a Perturbed Diamagnetic Medium

Pablo Ferrada[1], Génesis Serrano[2], Carol M. Ostojic[2], A Maureira[2], Manuel Zapata[2,3], Edward Fuentealba[1]
1. Centro de Desarrollo Energético Antofagasta (CDEA), Universidad de Antofagasta, Antofagasta, Chile
2. Laboratorio de Biotecnología Algal y Sustentabilidad, Universidad de Antofagasta, Antofagasta, Chile
3. Centro de Investigación Científico Tecnológico para la Minería, Universidad de Antofagasta, Chile
Corresponding author: pablo.ferrada@uantof.cl

1. Introduction

The effects of static magnetic fields (SMF) on living matter such as cell cultures and living organisms has been a promising research field. Efforts have been given in the understanding of the underlying mechanisms and interaction between the field and the biological system.

There are several examples where magnetism is present in living matter. For instance, the magnetotactic bacterium can align its body according to the Earth's magnetic field. This feature is possible due to chains of single-domain, biogenic magnetite (Fe_3O_4) to sense geomagnetic field [1].

Macroscopic organisms, namely birds, are known to orient themselves to magnetic field lines and thus travel long distances [2]. In fact, all materials fall into one of these categories, namely, diamagnetism, paramagnetism, ferromagnetism, ferrimagnetism or antiferrimagnetism [3].

At most fundamental level, the dipole magnetic moment is the quantity determining to a large extent the magnetic properties of molecules, atoms, ions, nucleus and subatomic particles. For electrons, it is quantized through the Bohr Magneton [4].

Biological cells exhibit a magnetic fingerprint depending on species. Researchers in [5] used this property to distinguish cells of several types by applying an external magnetic field from permanent magnets. The principle was based on the equilibrium between the magnetic gradient force and gravity.

Further investigations developed a magnetic trap for living cells in a buffer. In order that cells move towards zones of magnetic field minima, a paramagnetic fluid was added to the original medium and thus to achieve a magnetic susceptibility much higher than that of the cells [6].

Regarding effects of SMF on cells, authors showed an increased number and size of holes on cell membrane [7]. Thus, the volume force due to magnetic gradient led to higher membrane permeability.

The magnetic gradient mentioned above was examined by [8] where the discussion was centered on the mechanism by which magnetic fields act on living tissue. It was argued that it is the high magnetic gradient and not the field itself what can cause several effects in biological cells and their functions. They show that the high magnetic field gradient (HMFG) can be involved in the change of the ion-channel on/off probability, suppression of cell growth by magnetic pressure, magnetically induced cell division and cell reprograming, and forced migration of membrane receptor proteins.

Authors in [9] performed an analysis based on 56 articles about the quality of reporting SMF and treatment parameters. The found that 61% of the studies failed to provide enough experimental details about SMF. Consequently, the possibility for other researchers to replicate protocols and give satisfactory explanations might be reduced.

In this work we study cell cultures, specifically microalgae, subjected to SMF; both experimentally by implementing different set ups in the laboratory as well as performing experimental measurements, and numerically by modeling with COMSOL Multiphysics®. The importance of modeling and the simulation results resides in understanding experimental conditions to which cells are subjected. The study was conducted for two different microalgae species (denoted as S1 and S2), where S1 grows in fresh water and S2 lives in seawater, both with nutrients added to the original medium.

In general terms, the approach to accomplish this goal involves several steps. First, the creation of a 3D geometry corresponding to the experiment in the lab (Figure 1). It consists of a ring of permanent magnets surrounding a glass flask filled with a medium for the cell culture. A thin pipe enters the top to inject bubbles in the liquid, which due to buoyancy, results in circulation of the fluid inside the flask.

We used geometrical parameters of the real flask and the actual material properties. To specify magnetization vector for each magnet, we performed experimental measurements of the field by using a Hall sensor. Based on the exact-analytical solution of the field for a single magnet, we determined the remnant flux density to be specified for the individual-specific magnet belonging to the ring of each flask in the laboratory.

The next step after geometry and material definition, parameters determination and error estimation, was to perform different computations consisting on the following. (1) Solving Maxwell equations of magnetostatics with the Magnetic Fields No Currents interface to determine the magnetic flux density and the force per unit volume due to the field gradient for the geometry and material properties. (2) Solving Navier-Stokes equations with the Bubbly Flow interface. (3) Solving Newton's motion equation with the Fluid Particle Tracing interface to track the movement of biological cells (microalgae).

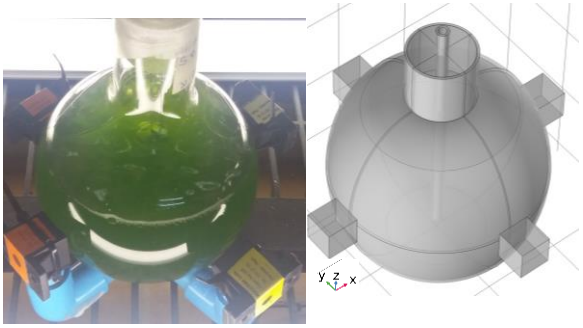

Figure 1. Left: Glass flask with an array of permanent magnets and a thin pipe to introduce air. Right: Geometry model in 3D.

Figure 1 shows the real and geometrical model of a glass flask surrounded by an array of permanent magnets. The flask is filled with a medium for a cell (microalgae) culture. A pipe enters the top through which there is an inflow of air to inject bubbles, which due to buoyancy lead to circulation of the fluid.

2. Theory and governing equations

2.1 Electromagnetism

The nature of the problem is the case when magnetic field is time-invariant. As a consequence, $\partial \boldsymbol{D}/\partial t = 0$, the magnetic field strength $\boldsymbol{H}$ and the flux density $\boldsymbol{B}$ can be expressed through Maxwell equations, Eq. 1 and Eq. 2.

$$\nabla \times \boldsymbol{H} = \boldsymbol{J} \quad (1)$$
$$\nabla \cdot \boldsymbol{B} = 0 \quad (2)$$

Equations 1 and 2 together with constitutive equations, initial and boundary conditions (BC) form a system of partial differential equations leading to a solution of $\boldsymbol{B}$ in space. Considering materials and media, two cases are distinguished. First, the field inside a permanent magnet, and second, the field in the medium outside the magnet. Equation 3 applies to a permanent magnet, for which $\boldsymbol{M}$ is the magnetization and μ_m is the magnetic permeability of the magnet material. For the region outside the magnet, assuming isotropy and linear magnetic medium, Eq. 4 holds, where μ_i is the magnetic permeability of medium *i*.

$$\boldsymbol{B} = \mu_m(\boldsymbol{H} + \boldsymbol{M}) \quad (3)$$
$$\boldsymbol{B} = \mu_i \boldsymbol{H} \quad (4)$$

There are mainly two approaches to find magnetic fields in space. (i) The vector potential ($\boldsymbol{A}$) and (ii) the scalar potential (φ). While (i) is associated to the molecular current, (ii) corresponds to the magnetic charge point of view. The introduction of $\boldsymbol{A}$ or φ into Maxwell equations leads to the set of differential equations to be solved associated to (i) or (ii), resp.

The use of the vector potential $\boldsymbol{A}$ allows finding the field for a single magnet that satisfies Eq. 1 and Eq. 2. Thus, the flux density can be written in terms of $\boldsymbol{A}$ as Eq. 5 shows. This relation always holds, as the gradient acting on the curl of a vector field is zero.

$$\boldsymbol{B} = \nabla \times \boldsymbol{A} \quad (5)$$

2.1.1 Single magnet

The components of the magnetic flux density $\boldsymbol{B}$ at any given point (x, y, z) away from the permanent magnet of given dimensions homogeneously magnetized along the z-direction, i. e. $\boldsymbol{M} = M_0\,\hat{k}$, can be found by evaluating analytical expressions of [10; 11]. The value of M_0 is related to the remanent flux density B_r through $B_r = \mu_m M_0$, in which μ_m is the magnetic permeability of the magnet material. A Hall sensor allows for determining the $norm\,\boldsymbol{B}$ and thus accesing to B_r and M_0 based on the analytical expressions for a single magnet. The calculated B_r values can be used in numerical analysis for finding $\boldsymbol{B}$ due to many magnets, as each individual magnet was characterized in terms of magnetization via B_r.

2.1.2 Many magnets

To find magnetic fields in space for an array of magnets, the scalar potential φ can be used. If no currents are considered, the curl of the magnetic field is zero (Eq. 1). In this case, $\boldsymbol{H}$ can be expressed in terms of φ according to Eq. 6. This approach applied to the magnets and their surroundings requires knowing their geometrical characteristics, specification of the solution region for computation, the magnetization vector $\boldsymbol{M}$ (or remanent flux density vector, $\boldsymbol{B_r}$), the *B*-*H* relationship and appropriate BC for each specimen of the array. In addition, the solution for the field in space outside the magnets depends on the magnetic permeability of that medium. This treatment of the magnetic field can be solved with the AC/DC interface [12].

$$\boldsymbol{H} = -\nabla\varphi \quad (6)$$

2.1.3 Boundary conditions

Finding numerical solutions to vector and scalar potentials requires specifying appropriate boundary conditions (BC), constrains and initial values. For magnetostatics, the BC $\boldsymbol{n_2} \cdot (\boldsymbol{B_1} - \boldsymbol{B_2}) = 0$ always holds between media 1 and 2 ensuring continuity to the normal component of $\boldsymbol{B}$. When scalar potential is introduced to find $\boldsymbol{B}$, zero magnetic potential, $\varphi = \varphi_0 = 0$, can be defined at convenient boundaries. Finally, numerical solutions require specifying the solution region, for which magnetic insulation condition $\boldsymbol{n} \cdot \boldsymbol{B} = 0$ is used.

2.2. Fluid dynamics

An air inflow is entering through a thin pipe near the bottom of the flask, resulting in bubbles which through buoyancy lead to fluid circulation. The continuity and momentum conservation are expressed by Eq. 7 and 8.

$$\frac{\partial}{\partial t}(\Phi_l \rho_l + \Phi_g \rho_g) + \nabla \cdot \left(\Phi_l \rho_l \boldsymbol{u_l} + \Phi_g \rho_g \boldsymbol{u_g}\right) = 0 \quad (7)$$

$$\Phi_l \rho_l \frac{\partial}{\partial t}\boldsymbol{u_l} + \rho(\boldsymbol{u_l} \cdot \nabla)\boldsymbol{u_l} = \nabla \cdot [-p\boldsymbol{I} + \boldsymbol{\tau}] + \rho \boldsymbol{g} + \boldsymbol{f_m} \quad (8)$$

Where Φ, ρ, $\boldsymbol{u}$, p, $\boldsymbol{I}$, $\boldsymbol{\tau}$, $\boldsymbol{g}$ and $\boldsymbol{f_m}$ are respectively the volume fraction, density, velocity vector, pressure, identity matrix, the viscous stress tensor (see [13]) and the magnetic gradient force (Eq. 9). The subindex l corresponds to liquid phase, whereas g stands for gas.

The magnetic gradient force acting on water has the form indicated in Eq. 9 where χ_v is the volume magnetic susceptibility of the fluid and μ_0 is the magnetic permeability of vacuum. The magnetic susceptibility and magnetic permeability are related through Eq. 10.

$$\boldsymbol{f_m} = -\chi_v \frac{(\boldsymbol{B} \cdot \nabla)\boldsymbol{B}}{\mu_0} \quad (9)$$

$$\mu_r = \frac{\mu_i}{\mu_0} = \chi_v + 1 \quad (10)$$

2.3. Particle tracing

Newtons' law for calculating the motion of cells (microalgae) due to the drag ($\boldsymbol{F_{drag}}$), gravity ($\boldsymbol{F_g}$) and magnetic gradient force ($\boldsymbol{F_m}$) are expressed by Eq. 11-14. In this case $\boldsymbol{F_m}$ is acting on cells in a fluid medium and thus one must consider the difference between magnetic susceptibility of microalgae and water. All forces are given in N. Therefore, the cell volume V_{cell} appears in Eq. 14.

$$\frac{d}{dt}(m_{cell}\boldsymbol{v_{cell}}) = \boldsymbol{F_{drag}} + \boldsymbol{F_g} + \boldsymbol{F_m} \quad (11)$$

$$\boldsymbol{F_{drag}} = \frac{1}{\tau_{cell}} m_{cell}(\boldsymbol{u_l} - \boldsymbol{v_{cell}}) \quad (12)$$

$$\boldsymbol{F_g} = m_{cell}\boldsymbol{g}\left(\frac{\rho_{cell} - \rho_l}{\rho_{cell}}\right) \quad (13)$$

$$\boldsymbol{F_m} = (\chi_{cell} - \chi_v) V_{cell} \frac{(\boldsymbol{B} \cdot \nabla)\boldsymbol{B}}{\mu_0} \quad (14)$$

The quantities m_{cell}, $\boldsymbol{v_{cell}}$, τ_{cell} and ρ_{cell} are the cells' mass, velocity, response time [13] and density, whereas ρ_l stands for the density of the liquid phase.

3. Methodology

3.1 General steps

The general procedure consists of three parts.

- Step 1: stationary study of *Maxwell* equations applied to magnetostatics to solve $\boldsymbol{B}$ for an array of magnets [12]. This problem was solved in 3D with the Magnetic Fields No Current (mfnc) interface within the AC/DC module.
- Step 2: time-dependent study of *Navier-Stokes* equations applied to a multiphase bubbly flow to solve velocity and pressure fields of liquid and gas phase, coupled with $\boldsymbol{B}$ [13; 14]. This part of the problem was solved in 2D with the Bubbly Flow (bf) interface of the CFD module.
- Step 3: time-dependent study of *Newton*'s law for fluid particle tracing (microalgae), coupled with the velocity field [15]. The visualization of microalgae movement was performed in 2D by using the Particle Tracing for Fluids (fpt).

3.2 Strategy

To determine whether the flow in study 2 is laminar or turbulent, the Reynolds (Re) number was calculated according to Eq. 15, where ρ_l is the fluid density, U and L are a characteristic fluid velocity and length, respectively, and μ_w is the dynamic viscosity of the fluid (water) [14].

$$Re = \frac{\rho_l U L}{\mu_w} \quad (15)$$

To find out which kind of coupling is needed between study 1 and 2, the magnetic Reynolds number (Re_m), defined according Eq. 16, was computed [16].

$$Re_m = \frac{UL}{\lambda} \quad (16)$$

The value of λ is the magnetic diffusivity equal to $(\mu_0\sigma_i)^{-1}$ where μ_0 and σ_i are the magnetic permeability of vacuum and fluid conductivity.

3.1. Initial values, parameters and geometry

Experimental measurements fed the analytical solutions of a single magnet to find its characteristic parameters. The value of the remanent magnetic flux density for individual magnets was $B_r = 1.15 \pm 0.14$ T, corresponding to Neodymium magnets N33.

Initial conditions such as bubble diameter (d_{bub}) and inlet air velocity were obtained experimentally using ImageJ software and filming how bubbles move in the glass flask. Thus, mean values for d_{bub} and the inlet velocity were calculated. To use the particle tracing study and track microalgae trajectories, their size distribution was determined by analyzing images of the cells also with ImageJ software. The measured quantities used as initial or input values were $d_{bub} = 10.4 \pm 3.6$ mm and a bubble speed $u_{in} = 10$ cm/s.

Simulations were run for fresh and sea water, considering their values of density, viscosity, and conductivity as summarized in Table 1.

Table 1: The values used for simulation correspond to properties of fresh and sea water at 20 C° [17].

Parameter (units)	fresh water	Sea water
Density (kg/m^3)	998.2	1024.8
Dynamic viscosity (Pa s)	0.001002	0.001077
Conductivity (S/m)	5.5×10^{-6}	5

Replacing values in Eq. 15 and 16 for both fresh and seawater gives $Re > 10000$ and $Re_m \ll 1$, respectively. These numbers indicate that the fluid is turbulent, and that $\boldsymbol{B}$ is determined by the boundary conditions, but not the fluid flow. In other words, one-way coupling is needed between study 1 and 2, i.e. Eq. 9 is computed after study 1 is complete but the $\boldsymbol{B}$ field is not recalculated after each iteration.

Step 1 to find $\boldsymbol{B}$ was solved in 3D. Further steps for study 2 Bubbly Flow and 3 Particle Tracing were solved by creating a 2D axis symmetric geometry from study 1 (Figure 2).

The cell species under study exhibit a diameter of $d_{cell,S1} = 9.6 \pm 1.6$ µm and $d_{cell,S2} = 10 \pm 1.3$ µm. Their densities are close to that of water, i.e $\rho_{cells} = 1090$ kg/m^3. The density value used for simulations corresponds to that of species 2 (S2).

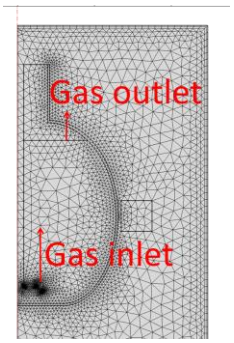

Figure 2. 2D axis symmetric geometry for bubbly flow (study 2) and particle tracing (study 3).

4. Results and discussion

The magnetic flux density for two different magnet configurations are illustrated in Fig. 3 for the case when all north poles are pointing the center of the flask, and in Fig. 4 for the case when two magnets with north poles are pointing the center and two magnets with south poles are oriented to the center of the flask. The arrow lines reveal the direction of the $\boldsymbol{B}$ field, while the surface plot shows its magnitude.

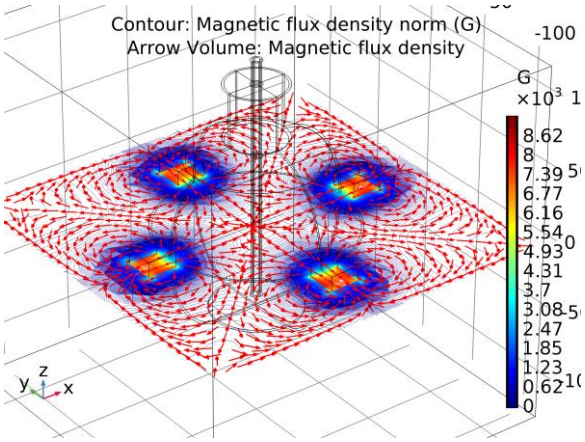

Figure 3. Contour plot and arrows for the magnet configuration consisting on all north poles pointing the center of the flask.

The two magnet configurations are discussed in the following. The case of all north poles oriented to the center leads zero magnitude of $\boldsymbol{B}$ at the center of the flask at z=0. On the contrary, the case where two north poles are pointing the center and two south poles are oriented to the center results in a minimum close to 100 G. For both configurations, the magnitude of the partial derivatives of the $norm\ \boldsymbol{B}$ with respect to x, y and z in the corresponding x, y and z directions are similar with values ranging from 40 G/mm down to 10 G/mm in the first 20 mm from each wall, and between 5 G/mm to 0 G/mm from the center to the flask to ¼ of the radius towards the flask walls.

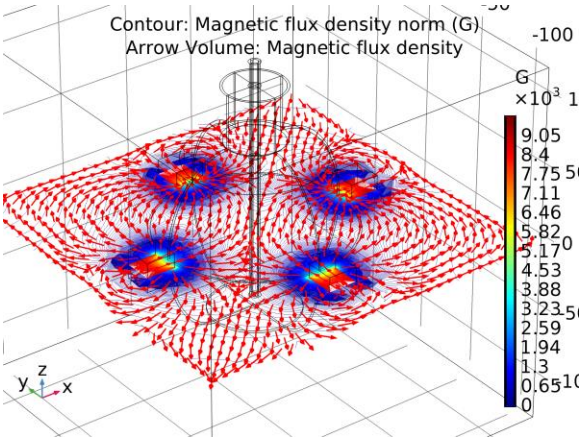

Figure 4. Contour and arrows for the magnet configuration consisting on two north poles (field lines coming out) pointing the center and two south poles (field lines entering) oriented to the center of the flask.

The measurements of the field with the Hall sensor allowed for comparing values of the magnetic flux density norm at the side of the magnet along magnetization axis with the numerical calculations. It was found that the relative error for the magnetic flux density norm ranged between 1.8% and 8%.

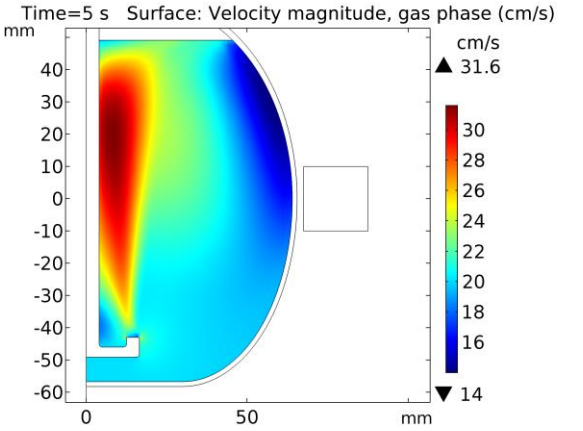

Figure 5. Surface plot of the velocity magnitude for the gas phase at 5 s of the simulation time.

Figure 5 shows the velocity magnitude for the gas phase. As air is continuously pumped into water, bubbles form and move due to buoyancy from the opening near the bottom (at a height of -45 mm) towards the top of the flask. The central part of the flask shows maximum velocity values reaching 31.6 cm/s, whereas velocities in zones close to the wall are as slow as 14 cm/s. Because of this process, water circulates in the flask (see Fig. 6 and Fig. 7).

Figure 7 and Fig. 8 depict the magnetic gradient force and liquid phase velocity for cells in fresh water and seawater, respectively. The key quantity determining how magnetic flux density ***B*** interacts and affects the fluid, via the magnetic field gradient, is the volume susceptibility χ_v of seawater and fresh water, respectively (denoted as $\chi_{v,sw}$ and $\chi_{v,pw}$). Authors in [18] used in their research a positive χ_v value for seawater, $\chi_{v,sw} = 400 \times 10^{-6}$ to perform a sensitivity analysis on magnetic susceptibility. The susceptibility value for fresh water is negative, $\chi_{v,pw} = -9.035 \times 10^{-6}$ [8].

As a result, the arrow lines showing the direction of the magnetic gradient force acting on water are starting from the magnet for fresh water and ending in the magnet for the seawater case. In both cases, the highest field intensity is found close to the magnet; however, the volume force due to magnetic field gradient in seawater is around 3 orders of magnitude higher than in fresh water.

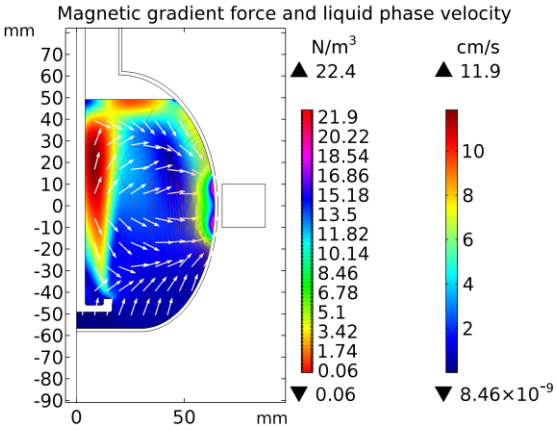

Figure 6. Arrows showing direction of magnetic gradient force acting on fresh water (S1) and a surface plot of the velocity magnitude for the liquid phase at 5 s.

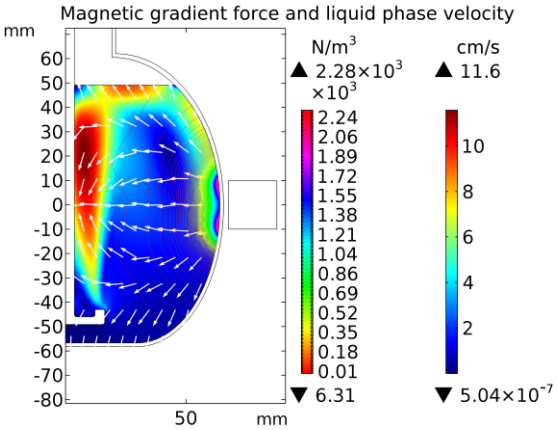

Figure 7. Arrows showing direction of magnetic gradient force acting on seawater (S2) and a surface plot of the velocity magnitude for the liquid phase at 5.

Regarding liquid phase velocity, differences for fresh water and seawater are less than 0.5 cm/s in terms of maximum velocity. This result means that

regardless the chemistry of water and the utilized ***B*** fields of this work, velocity values are similar in both cases. Nevertheless, the way the magnetic field interacts with water goes beyond this outcome, since viscosity and surface tension can change in presence of magnetic fields due to the formation of clusters with stronger intermolecular hydrogen bonds [19].

Conclusions

The combination of Magnetic Field No Currents (*mfnc*), turbulent bubbly flow (*bf*) and fluid particle tracing (*fpt*) succeed in modelling cell culture subjected to an array of permanent magnets. One-way coupling was used to solve Navier-Stokes equations for the bubbly flow with a user defined external volume force due to the magnetic field gradient. The 3D solution of the magnetic flux density ***B*** provided insights about its magnitude, direction and shape. Two different magnet configurations were selected for this simulation. The fluid dynamics problem was solved in a 2D axis symmetric geometry obtained from the original 3D model.

References

1. R. Nadkarni, S. Barkley, C. Fradin Nadkarni. A Comparison of Methods to Measure the Magnetic Moment of Magnetotactic Bacteria through Analysis of Their Trajectories in External Magnetic Fields. *Public Library of Science* **8**:12 e82064, 1-12 (2013).

2. A. Guenther, A. Einwich, E. Sjulstok, R. Feederle, P. Bolte, K.-W. Koch, I. A. Solov'yov, and H. Mouritsen. Double-Cone Localization and Seasonal Expression Pattern Suggest a Role in Magnetoreception for European Robin Cryptochrome. *Current Biology* **28**, 1–13 (2018).

3. J. Dobson. Chapter 4: Magnetic Properties of Biological Material. In *Handbook of Biological Effects of Electromagnetic Fields: Bioengineering and Biophysical Aspects of Electromagnetic Fields*. 3rd Ed. F. S. Barnes, B. Greenbaum, CRC Press (2006).

4. P. J Mohr and B. N. Taylor. CODATA recommended values of the fundamental physical constants:1998. *Reviews of Modern Physics* **72**: 2, 351-495 (2000).

5. N. G. Durmus, H. C.Tekin, S. Guven, K. Sridhar, A. Arslan Yildiz, G. Calibasi, I. Ghiran, R. W.Davis, L. M. Steinmetz, U. Demirci. Magnetic levitation of single cells. *Proc Natl Acad Sci USA* **112**: 28, E3661–8 (2015).

6. A. Winkleman, K. L. Gudiksen, D. Ryan, and G. M. Whitesidesa. A magnetic trap for living cells suspended in a paramagnetic buffer. *Appl. Phys. Lett*. **85**:12, 2411-2413 (2004).

7. Y. Liu, H. Qi, R. G. Sun, W. F Chen. An investigation into the combined effect of static magnetic fields and different anticancer drugs on K562 cell membranes. *Tumori* **97**:3, 386–92 (2011).

8. V. Zablotskii, T. Polyakova, O. Lunov & A. Dejneka. How a High-Gradient Magnetic Field Could Affect Cell Life. *Nature Scientific Reports* **6**:37407 (2016).

9. A.P. Colbert, H. Wahbeh, N. Harling, E. Connelly, H. C. Schiffke, C. Forsten, W. L. Gregory, M. S. Markov, J. J. Souder, P. Elmer and V. King. Static magnetic field therapy: a critical review of treatment parameters. *Evid Based Complement Alternat Med*. **6**(2):133–9 (2009).

10. Z J Yangt, T. H. Johansent, H. Bratsbergt, G. Helgesent and A. T. Skjeltorpt, Potential and force between a magnet and a bulk Y1Ba2Cu3O7-δ superconductor studied by a mechanical pendulum. *Supercond. Sci. Technol*. **3** 591497 (1990).

11. J. M. Camacho and V. Sosa. Alternative method to calculate the magnetic field of permanent magnets with azimuthal symmetry. *Revista Mexicana de Física* **E59,** 8–17 (2013).

12. AC/DC Module User's Guide, COMSOL v5.3a.

13. CFD Module User's Guide, COMSOL v5.3a.

14. C. Crowe, M. Sommerfeld, Y. Tsuji, Multiphase Flows with Droplets and Particles, CRC Press, 1998.

15. Particle Tracing Module User's Guide, COMSOL v5.3a.

16. P. A. Davidson. *An Introduction to Magnetohydrodynamics*. Cambridge University Press (2010).

17. ITTC – Recommended Procedures. Fresh Water and Seawater Properties (2011).

18. B. Baasch, H. Mueller, F. K. J. Oberle and T. von Dobeneck. Inversion of marine multifrequency electromagnetic profiling data: a new approach to resolve surficial sediment stratification. *Geophys. J. Int.* **200**, 439–451 (2015).

19. E. J. L. Toledo, T. C. Ramalho, Z. M. Magriotis. Influence of magnetic field on physical–chemical properties of the liquid water: Insights from experimental and theoretical models. *Journal of Molecular Structure* **888,** 409–415 (2008).

Acknowledgements

Authors acknowledge the generous financial support provided by Centro de Desarrollo Energético Antofagasta (CDEA) of the Universidad de Antofagasta, the Programa Semillero de Investigación de la Univesidad de Antofagasta and FONDEF/IDEA/CONICYT project N° ID15I10487.